Change Detection for Environmental Monitoring Using Unmanned Aerial Vehicle (UAV) Imagery

By

Christopher Chavis[1]

A Final Project Report

Submitted to the Department of Geoinformation and Environmental Technologies

Carinthia University of Applied Sciences

In Fulfillment of the Requirements for the

Marshall Plan Scholarship

Of the Austrian Marshall Plan Foundation

Project Supervisors:

Dr. Gernot Paulus[2] (Lead)

Dr. Karl-Heinrich Anders[2]

Dr. Piotr Jankowski[1]

November 1st, 2012

[1] Department of Geography, San Diego State University, 5500 Campanile Dr., San Diego, CA, 92182-4493
[2] Department of Geoinformation and Environmental Technologies, Carinthia University of Applied Sciences, Europastrasse 4, A-9524 Villach, Austria

Table of Contents

I. Abstract

Change detection is a complex process that spans multiple fields and is comprised of numerous components. While change detection has been historically dominant in remote sensing and more recently video surveillance, it is also used in medical imaging and diagnostics, underwater sensing, driver assistance systems and others (Radke et al. 2005). There is a copious amount of scientific literature detailing the various remote sensing techniques and digital image processing steps involved in change detection, but there is a surprising dearth of literature tying all these components together. Performing an efficient change detection requires knowledge of all the various elements comprising it, so a conceptual model of change detection is first developed by reviewing pertinent scientific literature. Following this conceptual model, a change detection for elevation is conducted by comparing a Digital Surface Model (DSM) from airborne LiDAR with a DSM generated from Unmanned Aerial System (UAV) imagery using automated photogrammetry techniques. The original data and results are compared against independent reference data collected with a high grade GPS and laser range finder.

II. Motivation

Three dimensional Digital Surface Models have long been the domain of satellite and Light Detection and Ranging (LiDAR) imaging systems. Elevation change detection using DSMs is a relatively new field study that has also been dominated by LiDAR and satellite with applications in urban disaster response (Corbane et al. 2011) and coastal soil erosion (Young and Ashford 2006). With the development of new technology in aircraft imaging systems and software packages, generation of three dimensional surface models has become not only feasible, but efficient with light weight Unmanned Aerials Vehicles (UAV). This provides many advantages over more traditional methods because UAV's are easier to transport and deploy, less expensive to operate than LiDAR and satellite platforms and can potentially generate comparably accurate results. UAVs also possess the potential for very high spatial resolutions, higher than both LiDAR and satellite. Demonstrating the ability of DSMs generated from UAVs to perform accurate elevation change detection could open up many new research opportunities that were not feasible using LiDAR or satellite data.

III. Research Question

Can accurate elevation change detection be performed on airborne LiDAR using a digital surface model constructed from low altitude, digital camera, UAV imagery with automated photogrammetry techniques?

This study aims to perform an efficient change detection of elevation by comparing a LiDAR DSM of the Technology Park in Villach, Austria collected in 2011 to a DSM generated by automatic bundle block adjustment from digital camera imagery collected with a lightweight UAV of the same area in 2012. Both the original datasets and results are compared against independent reference data in the form of high grade GPS and a laser range finder to evaluate the accuracy of the change detection.

IV. Building a Conceptual Change Detection Model

This section of the report details a conceptual model of the change detection process based on findings in relevant scientific literature. Figure 1 on the following page shows the change detection model with all the necessary components. The following subsections mirror the steps of the model.

IV.i Defining the Study

There is a wide variety of applications for change detection. These applications can include remote sensing, but also numerous other applications across many fields, such video surveillance, medical diagnostics, civil infrastructure (Radke *et al.* 2005), forest ecosystems (Coppin and Bauer 1996), and disaster response (Hussain *et al.* 2011). As a result, it is important to first clearly define the research question(s) and their realm of application as this influences many steps further along in the process. For this study, we will focus primarily on change detection within the field of traditional remote sensing, but acknowledge that many of the processes discussed here are applicable to other fields. Within the general field of remote sensing there are numerous unique applications; the majority are encompassed by the concepts of *Land Use* and *Land Cover* change (Radke et al 2005, Singh 1989). *Land Use* change analyses how humanity's use of the land evolves, such as from agricultural to urban, or undeveloped to developed, while *Land Cover* change indicates natural alterations in the physical landscape such as vegetation recession, soil erosion, or changes in snow and ice cover. Ultimately, defining the study for change detection merely entails answering the Six W's, or **W**ho, **W**hat, **W**here, **W**hen, **W**hy and Ho**w**, in the context of remote sensing. Once these six questions have defined the study, the next step in the process can be tackled.

IV.ii Determining Scales

Once the study questions have been answered and the scope identified, the next crucial step is determining the scale of the study. Scale is a decidedly relevant aspect of any study, but its importance is often underplayed. Woodcock and Strahler (1987) note that temporal and spectral scales are just as important as the spatial and assert that scale comprises an integral role in planning remote sensing investigations. Coppin and Bauer (1996) assert that, "The appropriate selection of imagery acquisition dates is as crucial to the change detection method as is the choice of the sensor(s), change categories, and change detection algorithms. The problem has two dimensions: the calendar acquisition dates and the change interval length [temporal resolution]." Selecting the appropriate scales for research can be a daunting task, however, as the possible combinations of scales almost limitless. At a basic level, the appropriate scale for remote sensing is a function of the type of environment and kind of information sought (Woodcock and Strahler 1987). These two parameters should already be answered in the Six W's, thus significantly simplifying the selection process.

Selecting a temporal scale can be an intuitive process based on the information provided by "When" during the problem definition phase. Examining the change in crop health on an annual basis would require a temporal resolution fine enough to collect several data sets during the peak growing season every year. This concept of "anniversary dates" is crucial because it minimizes discrepancies in reflectance due to seasonal vegetation flux and sun angle

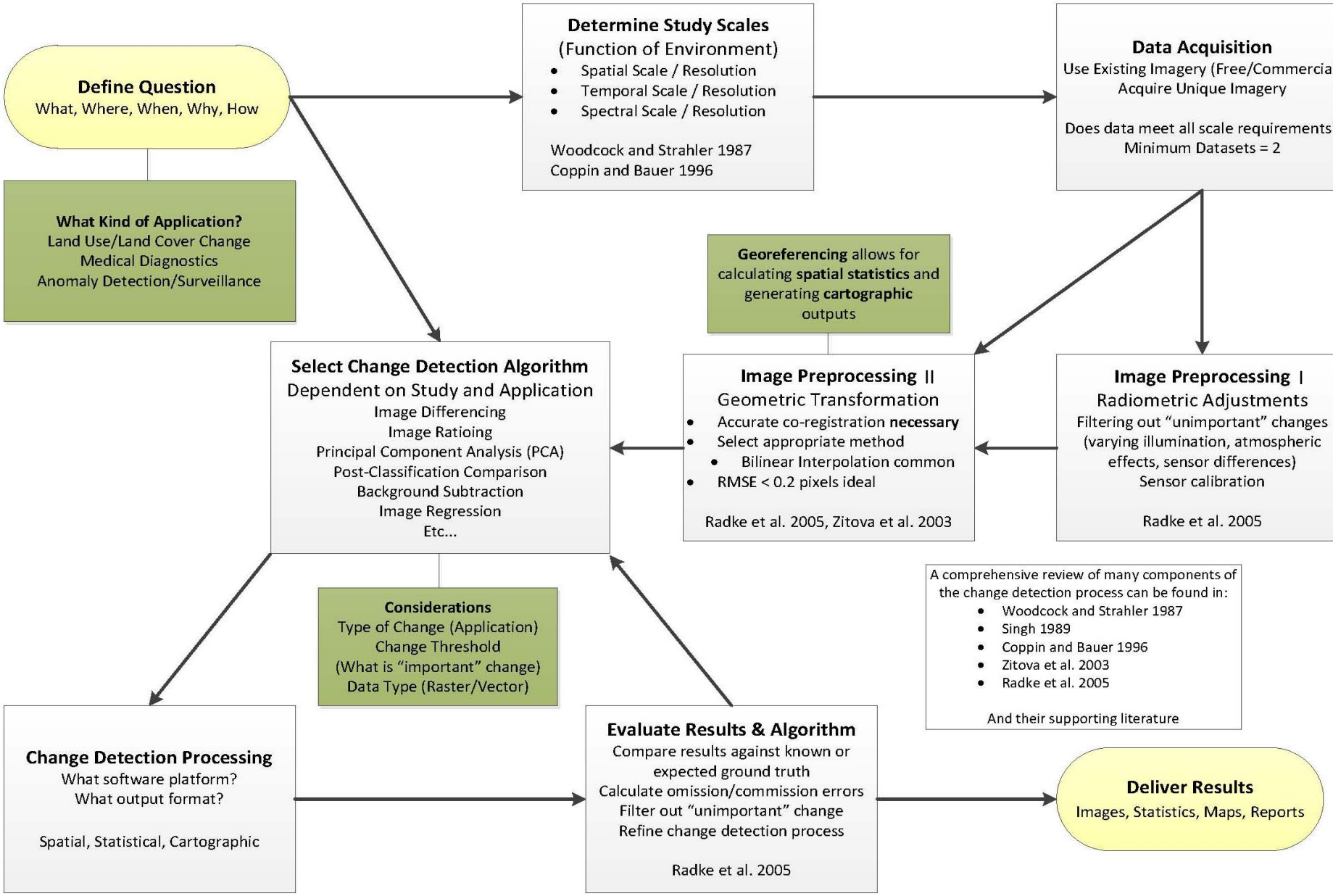

Figure 1 – Conceptual model for change detection workflow

differences (Singh 1989, Coppin and Bauer 1996). Thus, the temporal scale must be large enough to include the total range of study, but must be fine enough to compensate for atmospheric interference (clouds, etc.) that might obstruct the view of the scene. For instance, Landsat TM 7 images the same scene every 16 days and is archived for several years. This could

provide annual data sets during peak crop season, but if peak season is short and the few images acquired are cloudy, this could be problematic. It might be better to select a finer temporal resolution such as the SPOT satellite which images every 3 days. Thus, the chances of acquiring cloud free data in the peak crop season window every year increase. Not all studies have such strict temporal requirements however. Analysis of a specific event can have a simple temporal resolution of "before and after." Ideally the "before" and "after" datasets are as temporally close to the event as possible to assess the changes that directly result from the event, but in the case of disaster analysis, the event date cannot be predicted and the data must be acquired or collected within the expectations of the study.

Selecting a spectral scale is a simpler process than selecting a temporal one. The spectral requirements are again a function of environment and information sought and usually coincide with the information provided by "What." It simply becomes a case of deciding which portion(s) of the spectrum will be most useful. Taking again the example of examining crop health, the standard RGB spectrum combined with the infrared should be sufficient. With RGB/IR vegetation health can be analyzed with False Color Infrared and NDVI (Normalized Difference Vegetation Index). Monitoring wildfire spread and intensity changes might best utilize thermal sensors. A review of relevant literature can always assist with the selection of an appropriate spectral scale in case of uncertainty.

Selecting a spatial scale might be the simplest of all. Woodcock and Strahler (1987) have provided the remote sensing community with an essential study that indicates spatial resolution should be less than 0.5 of the size of the desired feature in areas of high local variance, or, where the environment varies a lot, such as urban settings. If a study is designed to derive information about features approximately one meter in size, a spatial resolution of 0.5 meters or finer would be desired. If local variance is low, in cropland for instance, a slightly coarser resolution can be acceptable. However, due to the vast improvements in spatial resolution capabilities and a massive increase in quantity and availability of sensors since the time of this article's publishing, acquiring data with the necessary spatial requirements is relatively easy and compromise is rarely required. Despite this, there is a tradeoff between temporal and spatial scales elucidated by Kennedy et al. (2009) that indicates finer spatial scales will lead to coarser temporal scales as less total area, or extent, is being covered by the sensor, thus requiring more time to repeat the image cycle. Coarser spatial resolutions permit grater spatial extent with each image capture, allowing for finer temporal resolutions.

IV.iii Data Acquisition

After defining the parameters and determining the necessary scales of the study, image and data acquisition can begin. This can be a difficult process and subject to compromise. There may not be an available sensor with all the desired scale requirements, or said sensor might be outside the budget of the project. A compromise in one or more resolutions might have to be made to select an appropriate, available sensor. Or, budget permitting, a sensor can be designed and implemented mission specifically. Designing mission specific sensors generally

restricts the remote sensing platforms to aerial imagery as opposed to satellite imagery due to the comparative ease of access. It should be noted that it is desirable to have all the data acquired from the same sensor to reduce the amount of required preprocessing before change detection.

Archived remote sensing data is abundantly available however, and can be readily used for many research questions. Continuing with the example of crop change analysis, NAIP (North American Imaging Project) is an aerial remote sensing project for monitoring crop health in the United States. Imagery was acquired during peak growing season every five years from 2003 to 2008 and every three years starting in 2009. The imagery is collected with one meter resolution in RGB and IR (in most states) and is collected with less than 10% cloud cover (USDA FSA 2012). This data is freely available and adequately satisfies the resolution and budget requirements of many crop change analyses (health, type, extent) over the recent decade. More specific and specialized studies might require more stringent sensor attributes and the design of a mission-specific imaging plan.

Because change detection is inherently a temporal question, it is imperative that there be multiple datasets. The minimum number of datasets required is two, but may contain several depending on the extent of the change being analyzed. These datasets are commonly referred to as the *imaged data* and *reference data* (Kennedy et al. 2009). *Image data* is relatively intuitive, referring to the imagery being analyzed in the change detection process and comprising the two dataset minimum. The type of image data acquired is dictated by the spatial, temporal and spectral scales defined previously and is integral to the design of the imaging sensor (Kennedy et al. 2009). Radar and LiDAR imagery are not as commonly used as optical imagery in landscape change detection, but are becoming more prominent in topographic change applications as the availability of airborne LiDAR increases (Kennedy et al. 2009). *Reference data* are categorized as independent sources of information that relate patterns in spectral space to real space or to evaluate the results of such a comparison (Campbell 1996). This can typically include other airphotos or ground measurements used for validation.

IV.iv Image Preprocessing

After the imagery has been collected, a certain amount of preprocessing must be undertaken to prepare the imagery for a change detection algorithm. The first of these, and the most critical, is geometric transformation. Geometric transformations are applied in image registration, a necessary step in all change detection problems (Radke et al. 2005, Kennedy et al. 2009). Image registration, specifically, is the process of overlaying two or more images of the same scene taken at different times, from different viewpoints, and/or different sensors (Zitova et al. 2003). In an ideal change detection situation, the imagery will be acquired from the same sensor to reduce the amount preprocessing required in the next step (radiometric adjustments) however, this is not always possible. There are myriad methods of image registration and geometric transformations for warping the “sensed” image to the “base” image. The majority of them require a user to manually identify common tie points between the two images, but there are automatic point matching tools for generating tie points. Zitova et al. (2003) provides a comprehensive review of image registration theory and practice, but gives special mention to one particular method noting that “the bilinear interpolation [method] is outperformed by higher-order methods in terms of accuracy and visual appearance of the transformed image, it

offers probably the best trade-off between accuracy and computational complexity and thus is the most commonly used approach" (p. 993). Accuracy of the image registration process is crucial for the accuracy of the change detection as it will reduce the number of false positives in the final result. Change detections assume that that unchanged pixels are spectrally stable and inadequate preprocessing can lead to an increase in false change detections (Kennedy et al. 2009). Townshend et al. (1992) indicates that registration values of 0.5 to 1.0 pixels are normally regarded as being satisfactory. Radke et al. (2005) asserts however, that an error margin of 0.2 pixel registration accuracy is necessary to keep misregistration error below 10%.

The second preprocessing step, while not as crucial as image registration, can improve the quality of the change detection in several situations. Radiometric adjustments seek to filter out "unimportant" changes from variation in radiance due to sun angle, atmospheric effects, and soil moisture (Radke et al. 2005, Singh 1989). Sensor calibration and normalization can also reduce the influence of data from different sensors and minimize atmospheric effects. Coppin and Bauer (1996) assert that radiometric calibration is essential for conducting change detections of vegetation. Alternatively, some change detection algorithms compensate for variations in illumination without the need for explicit preprocessing (Radke et al. 2005). Some radiometric adjustments include intensity normalization, homomorphic filtering, illumination modeling, and linear transformations of intensity as described by Radke et al. (2005). Speckle is a noise-like artifact and coherence effect commonly found in Radar imagery and a summary of research dealing with its suppression and removal can be found in Touzi (2002).

IV.v Algorithm Selection

There is a vast quantity of change detection techniques and algorithms available for temporal change analyses and selecting an appropriate one can be a daunting task and depends on the type of change being examined. Despite this, the process can be simplified in several ways. Kennedy et al. (2009) asserts that despite the variety of methods, most change detection methods contain a modeling (functioning algorithm) phase and a subtraction phase that compares dates via image algebra. The simplest and most widely used of these methods is univariate image differencing which subtracts Time 1 from Time 2 pixel by pixel providing a difference image indicating areas of change and the extent of the change (Singh 1989). Areas of little change will be close to 0 while areas of greater change will stray further. Less commonly used, but conceptually similar is image ratioing which divides corresponding pixel values (Singh 1989). If the values between times are consistent, their ratio will be close to one. Thus, the more significant the change, the further from one the ratio is. These techniques forego the modeling phase described above for change detection scenarios where less information is required about the type of change occurring. Bruzzone and Prieto (2000) categorize this type of change as *unsupervised* change which requires no prior user input. A *supervised* change detection by their definition would include the modeling phase described by Kennedy et al. (2009) where a user establishes example definitions for the change detection process. *Supervised* change detection techniques are more useful when "how" the scene has changed is important, such as examining urban growth and classifying what features began as and what they changed to. Malila (1980) simplify this distinction by dividing change detections into change measurement (stratification) and classification approaches.

A prime example of a *supervised*, or classification approach is Delta classification or "post-classification comparison" which utilizes independently produced spectral classification results from each image set followed by a pixel-by-pixel comparison to detect changes in cover type (Coppin and Bauer 1996). This technique has one major benefit in that it minimizes the problem of radiometric calibration because the imagery is independently classified. However, the accuracy of the change detection becomes dependent on the accuracy of the initial classifications. The sheer number of change detection techniques is vast and there a multitude of publications reviewing the majority of them including Singh (1989), Coppin and Bauer (1996), Mas (1999) and Radke et al. (2005), but Milne (1988) provides a convenient table grouping twelve major techniques into four categories ordered by complexity and required processing time.

Table 1 - Classification of digital change detection techniques (Milne 1988)

Complexity Groupings	Techniques
Linear Procedures	Difference images
	Ratioed images
Classification Routines	Post-Classification change detection
	Spectral change pattern analysis
	Logical pattern change detection
	Layered spectral/temporal change detection
	Radiance vector shift
Transformed Data Sets	Albedo difference images
	Principal component analysis
	Vegetation indices
Others	Regression analysis
	Knowledge-based expert systems

One important consideration to be made during the technique/algorithm selection phase is that of thresholding. Singh (1989) stresses that defining the boundary between "change" and "no-change" pixels is integral, especially for image differencing methods. This is reinforced by Coppin and Bauer (1996), Mas (1999), and Radke et al. (2005). Like selecting an appropriate algorithm and technique, selecting an appropriate threshold to separate change from no-change is a complicated process that varies with the selected change detection method and has several publications dedicated to it. Radke et al. (2005) indicates that the threshold is often chosen empirically and in depth discussions on selecting an appropriate threshold can be found in Rosin (2002), Rosin and Ioannidis (2003) and Smits and Annoni (2000). However, selecting a threshold can relatively easy and is directly related to the type of information sought by the study.

IV.vi Information Extraction and Evaluation

After defining the change detection parameters such as algorithm and threshold, the change detection can be processed and information extracted. This is usually performed with a GIS software such as ERDAS Imagine or ArcGis by ESRI, but there are many available and selection should be based on familiarity and ease of access. Most often, the information extracted is empirical and can be difficult to interpret in its raw form. The simplest form is a

binary map or "change mask" where 0 indicates no change and 1 indicates changes set by the threshold (Radke et al. 2005). However, stratified maps can also be generated categorizing changes by magnitude. This is useful for extracting additional information about how features have changed. Results from pixel-by-pixel change detections are typically noisy with isolated pixels and "salt and pepper" effects that can detract from statistical information extracted. The simplest methods for correcting these negligible changes (or errors) is filtering techniques, often using the median to "smooth" imagery by recalculate outliers based on their neighbors (Radke et al 2005).

Evaluation of the change detection is the final crucial step. It is not uncommon to evaluate the results and modify the change detections parameters, processing the change again. Errors in the change detection process are usually quantified statistically by comparing the change map to independent reference data at sample locations (Kennedy et al. 2009). To conduct a proper accuracy assessment, these independent data must be considered "truth" and collected without error (Kennedy et al. 2009). However, truth is not absolute and in practice, reference (and map) data is rarely perfect. Thus, it must be acknowledged that all data possesses a certain amount of error and evaluation of a study's accuracy must consider this, thus making analysis an evaluation of agreement rather than an assessment of accuracy (Kennedy et al. 2009).

V. UAV Imaging and Digital Photogrammetry

V.i Imaging with Unmanned Aerial Vehicles (UAV)

The term UAV (Unmanned Aerial Vehicles) applies to all airborne vehicles, with no onboard pilot, but with the capability of being controlled (Eisenbeiss 2004). This broad definition covers a wide range of craft. The simplest UAV's range from tethered balloons and blimps to more complex UAV's such as fixed-wing aircraft and helicopters (Everaerts 2008). The imaging capabilities of UAV's vary widely across different platforms. Each UAV has its own unique payload capabilities relative to its size and power. In addition, the sensor payload must be automatically or remotely operable, due to the lack of onboard personnel (Wegener and Schoenung 2005). However, remote sensing with UAV's is much more versatile compared to their piloted counterparts. UAV's have carried instruments that cover the whole spectrum of remotely sensed data (Everaerts 2008) allowing for the tailoring of sensor parameters appropriate to the mission. These sensors could range from simple off-the-shelf digital cameras (Everaerts 2008) to hyperspectral, 580 band sensors (Johnson *et al.* 2003) to thermal sensors (Ambrosia *et al.* 2003). In addition to variability in spectral resolution, UAV's also provide extensive flexibility in spatial resolution. Sensors can achieve anywhere from 5 centimeter resolution (Laliberte and Rango 2009) to 8 meter resolution (Ambrosia *et al.* 2003) and coarser.

Unmanned Aerial Vehicles are becoming a prominent alternative in remote sensing applications. The reason for this is threefold: UAV's are safer, more flexible, and more efficient than their piloted counterparts (Ambrosia *et al.* 2003, Everaerts 2008, and Laliberte and Rango 2009). This makes the application of UAV's preferable in many situations, but most importantly for time-sensitive disaster analysis. UAV's have been used to safely and efficiently monitor wildfires (Ambrosia *et al.* 2003), thunderstorms (Wegener and Schoenung 2005), earthquakes

(Hussain *et al.* 2011) and numerous other disasters such as floods, toxic spills, and volcanoes (Everaerts 2008). Efficient and flexible remote sensing in disaster situations can greatly improve rescue and relief efforts, damage assessment, and the pre-emptive planning of safeguard measures (Hussain *et al.* 2011).

One area where UAV's have been under-utilized is the generation and application of Digital Surface Models (DSMs) for volumetric analysis. Aerial LiDAR (Light Detection and Ranging) is the accepted standard for DSM generation (Gehrke *et al.* 2010) and DSMs have been generated using numerous satellite platforms including IKONOS and QuickBird (Eisenbeiss *et al.* 2004). These methods are very expensive however, and UAV's can provide efficient alternatives for the generation of 3D data. LiDAR and satellite platforms have typically been the preferred method of surface model generation due to their extremely high accuracy. UAV's are beginning to compete as the accuracy of their DSMs improves, because DSM accuracy is a function of ground resolution (flying height) of the input imagery (Jensen 2007, Strecha 2011, Küng 2011) and UAV's can achieve very high spatial resolutions from low altitude. 3D data from these DSMs can provide certain advantages over 2D imagery in disaster response. Some features and changes, such as soft-story failures where buildings collapse directly on top of weaker, lower floors, are undetectable in two dimensions from nadir (Corbane *et al.* 2011). Creating 3D surface models of disaster areas can overcome these obstacles in addition to providing the information obtained from 2D imagery.

V.ii Digital Photogrammetry

Photogrammetry is the "art, science and technology of obtaining reliable information about physical objects and the environment through the process of recording, measuring and interpreting photographic images and patterns of electromagnetic radiant imagery and other phenomena" (American Society of Photogrammetry 1980). Jensen (2007) describes it more succinctly as "the art and science of using aerial photography to make accurate measurements of ground features." Measurements such as scale, object length and height, and area can all be extracted from a single photograph. When analyzing overlapping aerial photographs (stereo) the precise planimetric location of a feature (x,y), and precise feature height (z) can be found. Most importantly for this study, digital photogrammetric techniques can be applied to generate 3D surface models from this information (Jensen 2007). In fact, the largest application of photogrammetry is the extraction of topographic information (Erdas 2010). But in order for terrain extraction to be effective (and accurate), the images must possess a certain amount of overlap. The minimum requirement for most applications is 20-30 percent overlap and sidelap (Jensen 2007), but effectiveness increases as the percentage increases. Some scenarios require extremely high overlap rates, over 80 percent, such as performing photogrammetry in extremely mountainous terrain (Jensen 2007). Multiple flightlines of overlapping imagery are referred to as a *block* of aerial photography (Jensen 2007).

A *bundle block adjustment* (BBA) is a specific digital photogrammetric technique used in the construction of three dimensional surfaces from overlapping image sets. It is a form of aerial triangulation that establishes a mathematical relationship between the images, the sensor model and the ground (Erdas 2010). Triggs et al. (2000) describe bundle block adjustment as a method of combining 3D feature coordinates with camera orientations and calibrations in a large, sparse, geometric parameter estimation. Essentially, a BBA combines every image with its

geolocation (GPS), exterior sensor information (pitch, roll and yaw), and interior sensor calibration (focal length, CCD size) into a mathematical relationship from which topography can be extracted. From the bundle block adjustment, 3D points are calculated and then interpolated to from a Triangular Irregular Network (TIN) which is then used to obtain a DSM (Küng et al. 2011). In addition to generating DSM, the internal and external camera parameters of the input imagery can be used to calculate the geometric transformation of the input images to the orthographic coordinate system (Strecha et al. 2008). This means that every pixel imaged during the flight is assigned to its correct planimetric (x,y) coordinate in real space, thus creating a paired, orthorectified mosaic of the scene.

VI. Methods: Implementing the Model

Following the conceptual model (Figure 1) outlined previously, Figure 2 represents the change detection model created specifically for this research project as a methods outline. The following subsections mirror the steps of Figure 1, but are adapted to the specifications of this research project.

VI.i Defining the Study

Defining the parameters of the study is the initial step as shown in Figure 2. First, the study can be defined within the field of general remote sensing as change detection of elevation using traditional remote sensing techniques involving airborne LiDAR, aerial imagery, digital photogrammetry and digital image processing. Secondly, this study is examining, specifically, changes in elevation, either natural or artificial thus making it a study of Land Use or Land Cover (LULC) change.

The second step is to define the Six W's of the study, though many of them are indirectly defined in the beginnings of a paper. At first glance, *Who* might seem irrelevant, but it is important to remember that research funding comes from somewhere and there is always someone with a vested interest in the study. This study has several associated parties. Funding comes from the Austria Marshall Plan Foundation, data acquisition is performed by Dr. Paulus and Dr. Anders of Carinthia University of Applied Sciences, the same institution that provides facilities for conducting the research. Research and data processing is conducted by Christopher Chavis of San Diego State University in conjunction with Carinthia University of Applied sciences.

Typically, defining *What* is a fairly easy step as it directly reflects the specific research question, which is usually already identified. In this case, *What* is a change detection of elevation using LiDAR and a DSM generated from UAV imagery with photogrammetry techniques. *When* is a very broad concept, but critical to place the study in the related literature. The LiDAR data was collected in 2011 and the UAV imagery collected on July 9th, 2012. GPS reference data was collected on July 24th, 2012 and laser range finder data was collected on August 7th, 2012. *Where* is also a critical piece of information. This study will utilize data centered around the Carinthia University of Applied Sciences in Villach, Austria. *Why* is a reflection of the motivation for the study, which is to demonstrate the ability of DSMs generated from UAV imagery for conducting elevation change detection against airborne LiDAR.

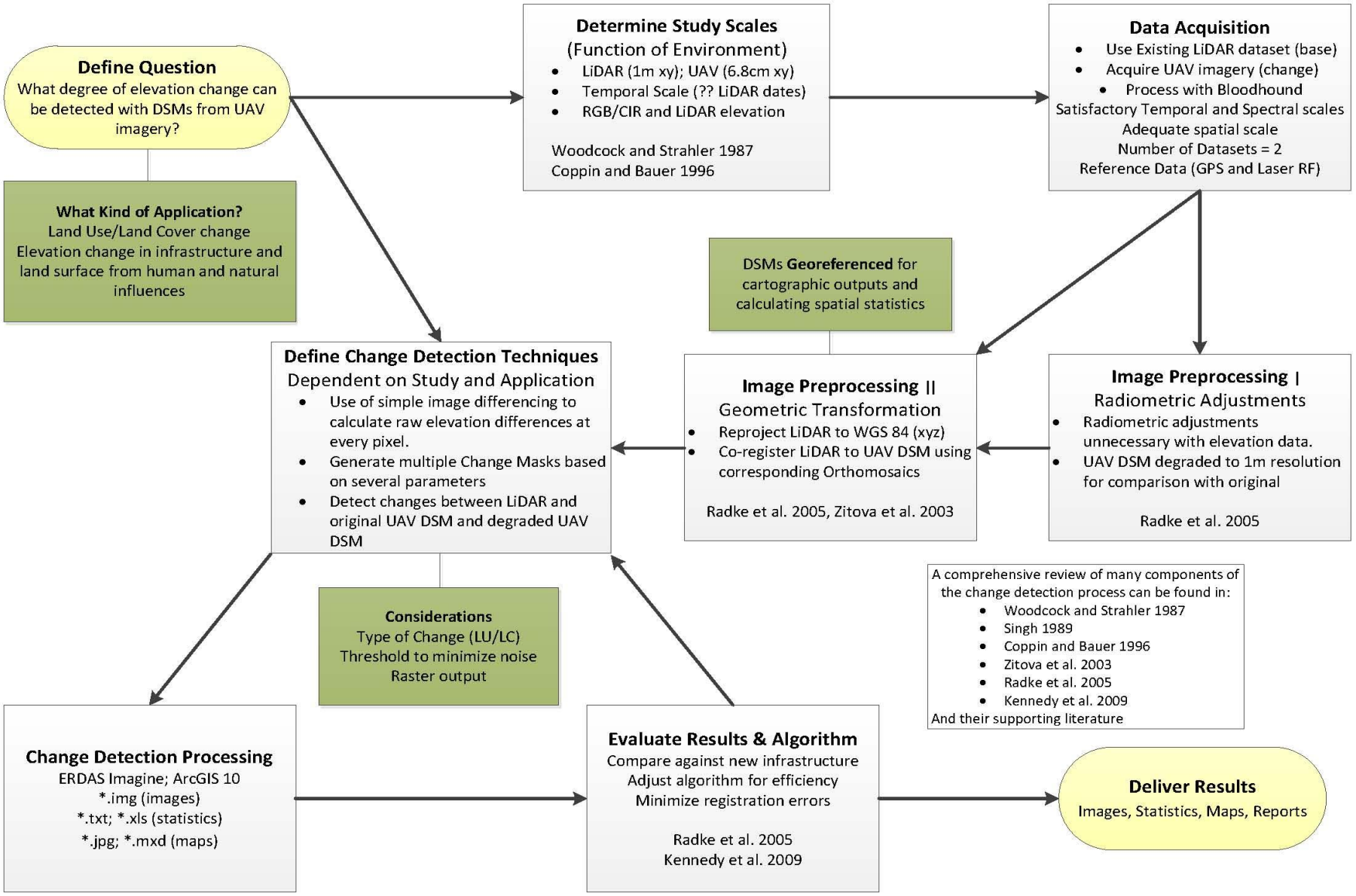

Figure 2 - Conceptual Change Model Applied to Project

If successful, it will provide a stable and attractive alternative to relying on airborne LiDAR for analyzing elevation information.

How is the final W and arguably the most important. The majority of *How* is detailed in the Methods of any study. In short, digital image processing using various software platforms will be utilized to compare the elevations of two co-registered DSMs (one from LiDAR, one from UAV imagery) against known ground truth measured with GPS and a laser range finder.

VI.ii Determining Scales

The next phase of the model in Figure 2 is determining the necessary scale requirements of the data for the study. Often times, as is the case with this study, spatial scales are determined by the data available. The lidar data of the area is available in 1 meter (interpolated) resolution and the UAV imagery, GPS points, and laser range finder were acquired with subdecimeter resolution. However, a study is only as good as its coarsest resolution, so the effective spatial resolution for this study is 1 meter. Temporal resolution is very coarse, approximately two years. However, this is beneficial due to the construction of several new buildings, or quantifiable elevation changes, during the interval. The spectral requirements of the study include RGB imagery for UAV DSM generation and orthomosaic generation which is necessary for registering the DSMs and a lidar scan for interpolating a DSM.

VI.iii Data Acquisition

Three principal datasets were acquired for this study: the base dataset, the change dataset and a reference dataset for accuracy assessment. The base dataset is a lidar DSM and accompanying orthomosaic. The lidar pointcloud was acquired in April, 2010 using a Riegl LMS Q680i. The point density during collection was 4 points per m^2 with a max point distance of 0.9 m. The data was then interpolated into a 1m DSM and georeferenced with the ORIENT-LIDAR software package using the WGS84 spheroid and ETRS89 datum with a horizontal positioning accuracy of ±30 cm and a vertical positioning accuracy of ±15 cm and projected using the Universal Transverse Mercator (UTM) projection in zone 33 North. From there, it was reprojected to the Austrian national datum of GK M31 with the Bessel spheroid and then provided to the Carinthia University of Applied Sciences in Villach.

The change dataset is a DSM and orthomosaic generated from low altitude, digital camera imagery acquired with a UAV. The imagery was acquired using a Lumix LX5 digital camera by Panasonic attached to the Low Cost Unmanned Imaging System (LOUIS) UAV designed by TerraPan Labs LLC. The flight plan for image acquisition was designed using F-PLANAR and implemented on July 9th, 20102. A total of 218 Images were acquired at 2 second intervals along 450m flight lines with a study width of 400m generating imagery with 60% overlap and 80% sidelap. Cruise altitude was set at 150m generating a pixel size of approximately 5.8cm. Total flight time for image acquisition took approximately 11.7 minutes with a cruise speed of 50 km/h. The Directifi software package was used to pair each image from the flight log with a GPS geotag from LOUIS' onboard GPS unit and export the image to TIFF format. LOUIS' GPS system recorded GPS data using the WGS84 spheroid and ETRS89 datum.

Two sets of reference data were collected to complement the change datasets. The first is a set of survey GPS points of the area and the second is a collection of building heights

measured with a laser range finder. A total of 56 Real Tike Kinetic (RTK) GPS points were collected on July 24th, 2012 using a Leica Geosystems GS08 receiver. Collected points were documented photographically to assist with future GCP identification. An accuracy report containing vertical and horizontal positional accuracies for every point was generated using Leica Geo Office 8.2. All 56 points were collected in WGS84 for comparison with the data collected from LOUIS and converted to MG K31 for comparison with the lidar data. 5 unique height readings for 5 building elevations were collected using a Leica Disto D5 laser range finder. Each building was measured twice from two different locations to ensure consistency.

VI.iv Product Generation Using Bloodhound

Product generation is a part of the data acquisition phase defined by step 3 in Figure 2. Bloodhound is an automatic BBA software program developed by Pix4D and licensed to TerraPan Labs LLC. It is specifically designed to automatically generate georeferenced 3-D surface models, georeferenced 3-D point clouds and orthomosaics from UAV imagery. Bloodhound's capability for generating 3-D point clouds distinguishes its potential for non-classical change detections. While it remained unused in this particular research project, the potential for comparing 3-D point clouds between elevation datasets adds a whole new dimension to classical change detections.

The only principle requirement for product generation with Bloodhound is that each input image must have an approximate geotag. Directifi was used to satisfy this requirement by tagging each image acquired during the flight with its corresponding geotag from LOUIS' onboard GPS unit. However, Bloodhound also allows for the inclusion and identification of GCPs to greatly enhance the accuracy of the resulting products. Bloodhound has been shown to provide results with 0.05-0.2 m accuracy with GCPs and 2-8 m accuracy without any manual intervention (Küng et al 2011). GCPs were selected from among the 56 survey GPS points collected during data acquisition.

Table 2 - Bloodhound GCPs

GPS Point #	XY Acc. (cm)	Z Acc. (cm)	# of Images
3	0.8	1.3	16
8	0.8	1.4	11
12	0.8	1.3	15
13	0.8	1.3	12
21	0.9	1.5	12
22	1.0	1.3	15
25	1.0	1.5	13
33	0.9	1.2	9
41	1.2	1.6	15
44	1.0	1.3	15
53	0.9	1.4	5
57	1.2	2.7	4

Sometimes, not all imagery collected during a flight is adequate or desirable in a BBA. Directifi possesses the ability to filter out imagery from a flight based on exterior orientation parameters (altitude, pitch and roll) and generate a .csv file formatted specifically for input into Bloodhound. For this study, Directifi was used to filter out all images taken below the altitude threshold of 140 meters, or 10 meters below the target altitude. This was done in order to closely preserve spatial resolution of the image block and resulting Bloodhound products. Of the 218 collected images, 140 were uploaded into Bloodhound along with their corresponding geotags and exterior sensor orientation parameters.

Once the 140 selected images were uploaded into Bloodhound, 12 GCPs were selected from among the 56 survey GPS points taken in the imaged area. Table 2 indicates which GPS points were used as GCPs, their GPS accuracy confidence and the number of images in the block each GCP was identified in. GCPs were selected based on their high degree of accuracy and their distribution throughout the study area. Once all the imagery and GCPs were loaded into Bloodhound, the GCPs were manually identified in the imagery.

VI.v Image Preprocessing

With all orthomosaics and DSMs generated, the project moved on to steps four and five of Figure 2. Image preprocessing was undertaken to prepare the data for change detection. Radiometric preprocessing (Image Preprocessing I) was bypassed for several reasons. The primary reason is that, being rasters comprised of elevation values, the DSMs to be analyzed in the change detection have no inherent radiometric value, thus rendering radiometric processing unnecessary. Additionally, the orthomosaics are only used for visual analysis of changes and for templates to co-register the digital elevation models. As a result, radiometric preprocessing would have been inefficient and unnecessary.

Geometric preprocessing (Image Preprocessing II) was extensive to prepare the DMSs for change detection. The first step was to project both data sets in the same coordinate system, horizontally and vertically. The lidar dataset was originally collected in 2010 using the ETRS89 datum for central Europe with the WGS84 spheroid. However, it was converted to GK M31 datum in the Bessel spheroid before being provided to the Carinthian University of Applied Sciences. LOUIS' onboard GPS unit collects GPS readings in the WGS84 spheroid and datum (referred to as ETRS89 in Europe) and Bloodhound outputs all results in WGS84, projected into UTM. As a result, the lidar and orthomosaic were reprojected horizontally back to WGS84 using ERDAS Imagine. Afterward being reprojected horizontally, the DSMs elevation was reprojected from the Bessel vertical datum to the WGS84 vertical datum.

Because both datasets were georeferenced prior to reprojection, they aligned very closely post-reprojection. However, to ensure their accurate alignment, the lidar was co-registered to the Bloodhound results. This process was done in ERDAS Imagine manually by identifying tie points between the two orthomosaics. The DSMs possess a very high degree of internal alignment accuracy with their corresponding orthomosaic. As a result, the orthomosaics can be used to co-register the DSMs. Ten tie points were identified between the two orthomosaics with a mean total RMSE of 0.14, sufficiently lower than the threshold of 0.2 recommended by Radke et al. (2005). A second order polynomial transformation model was applied using bilinear interpolation for resampling. The transformation model was then saved and applied to the DSMs to accurately co-register them.

VI.vi Algorithm Selection

Selecting an algorithm for step six (Figure 2) of the change detection model was a relatively simple process. The nature of the data and aims of the research question made the selection easy. The high accuracy of image registration (pixel alignment) and elevation data (pixel values) lent themselves well to simple image differencing. Simple image differencing will provide the raw elevation difference between the two datasets on a per-pixel basis which will be useful for quantifying the absolute elevation change between the two datasets.

There were some drawbacks to consider with the selection of simple image differencing. The main drawback worth mentioning is that in an idea change detection with simple differencing is that the value zero is the indicator of no change. Practically, this rarely occurs, so a threshold for "no change" has to be arbitrarily determined and applied. A vertical accuracy of ±15 cm with the lidar would set an instinctive change threshold at ±15 cm as well. However, due to variable terrain, multiple data reprojections, different data sources and a primary interest in detecting infrastructure changes, the initial change detection threshold was selected at ±1 m.

VI.vii Information Extraction and Evaluation

Two software platforms were used in step seven of Figure 2, or information extraction and evaluation. Simple binary change masks (0 for no change, 1 indicating change) were deemed insufficient for the study as they don't provide any indication of the degree of change that occurred. Consequently, stratified change maps were generated using both the ArcGIS 10.0 package (ArcMap and ArcScene) and ERDAS Imagine 2011. ArcMap was used to apply various classifications based on the raw change data for visual interpretation. ArcScene was used to render the DSMs and Orthomosaics in 2.5-D for visual comparison.

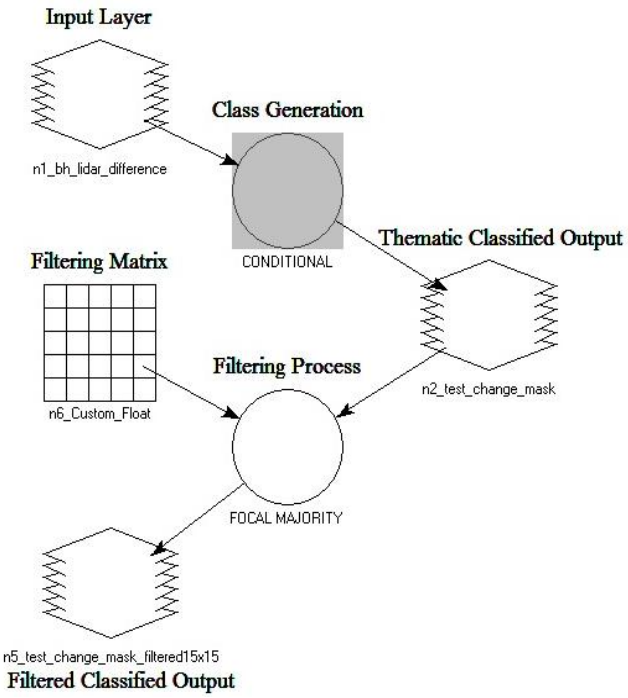

The Spatial Modeling toolbox within ERDAS Imagine 2011 was used to construct a model that received the DSM of difference values as an input and apply a stratified change mask followed by a smoothing filter with a classified, thematic output. Several class boundaries were tested as well as several smoothing techniques. Most class boundaries were established at integer accuracy to keep the contrasts between changed features sharp. Filtering methods consisted mostly of applying Focal Majority matrixes of various sizes. The construction of a model allows the user to quickly adjust change thresholds and smoothing techniques and rerun the process thereby generating multiple change masks for side-by-side comparison.

Figure 3 - Change Mask Classification and Filtering model for ERDAS Imagine 2011

Overall, the change algorithm was deemed satisfactory and information extraction techniques performed well. A full discourse on the effectiveness of the change masks and filtering methods will be given in the Discussion section.

VII. Results

The results of this study can be divided into two general categories: imagery and statistics, or qualitative and quantitative data, respectively. Here, only the data is presented. Analysis and discussion of the results will follow in the subsequent section.

Figure 4 - Bloodhound Orthomosaic over LiDAR Orthomosaic with GPS point (red) reference data

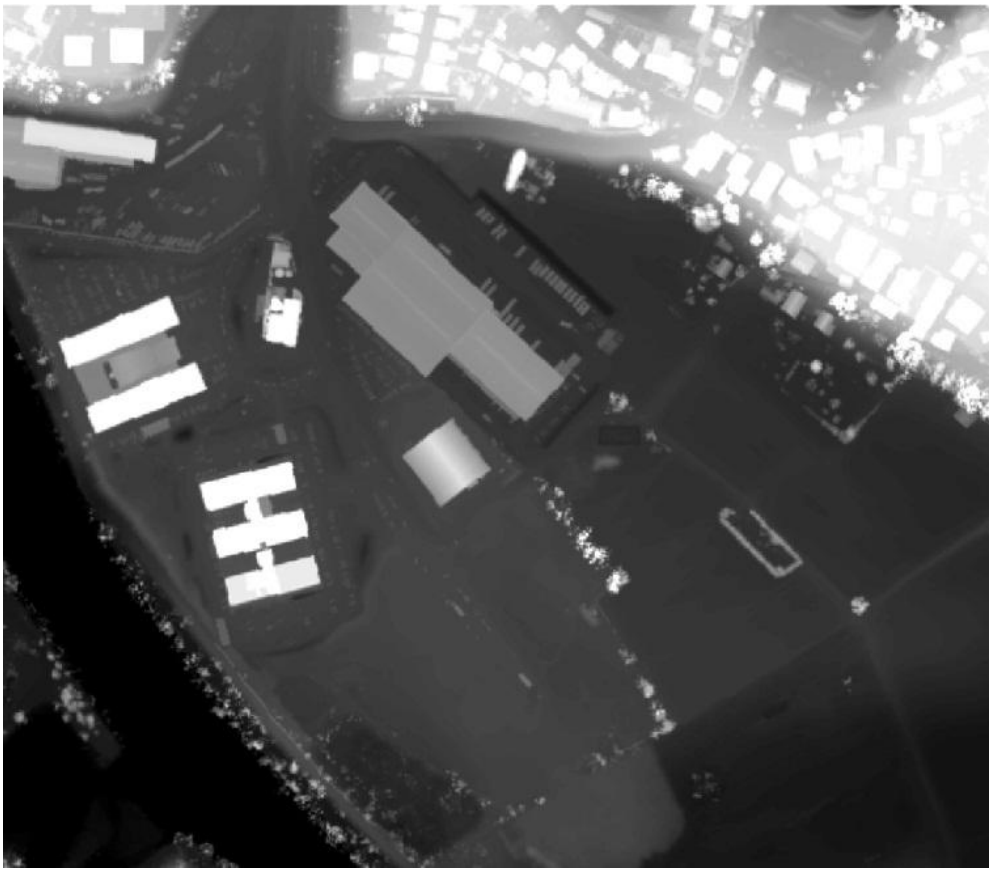

Figure 5 – LiDAR DSM (1m XY resolution)

Figure 6 – Bloodhound DSM (0.068m XY resolution)

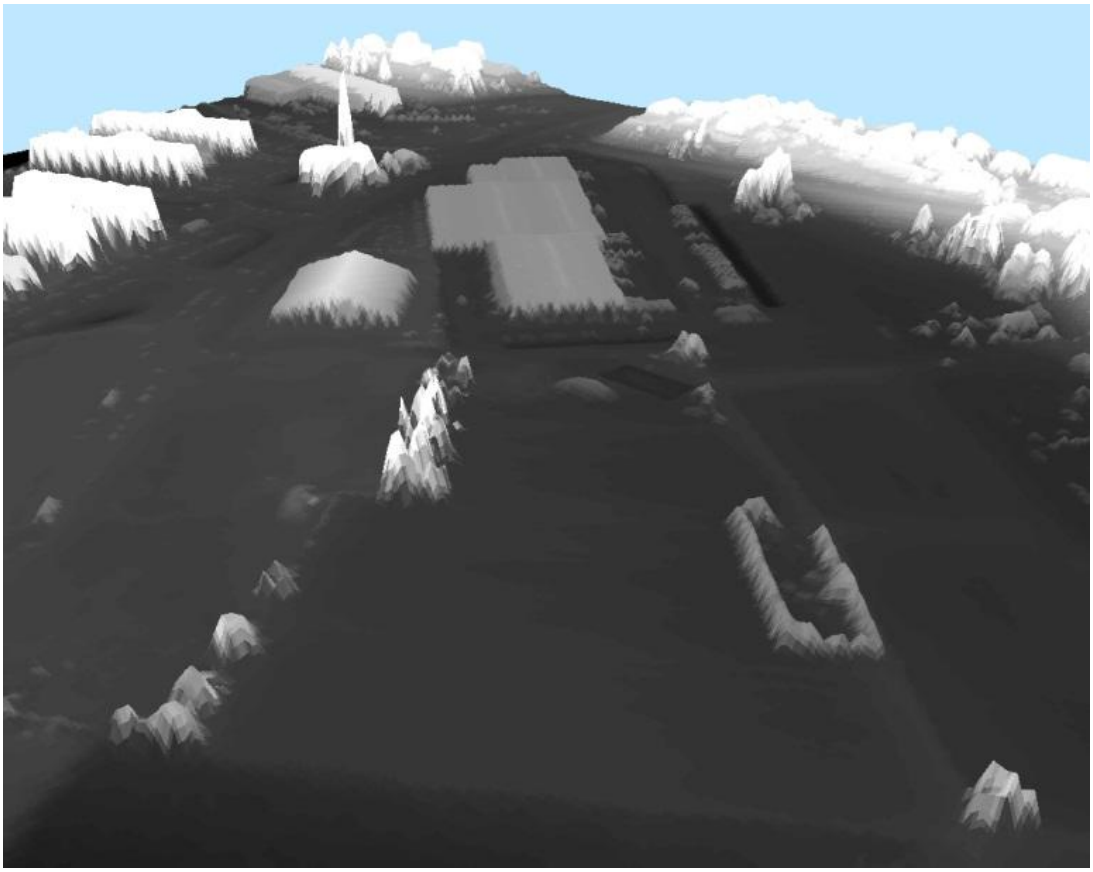

Figure 7 – LiDAR DSM rendered in 3D

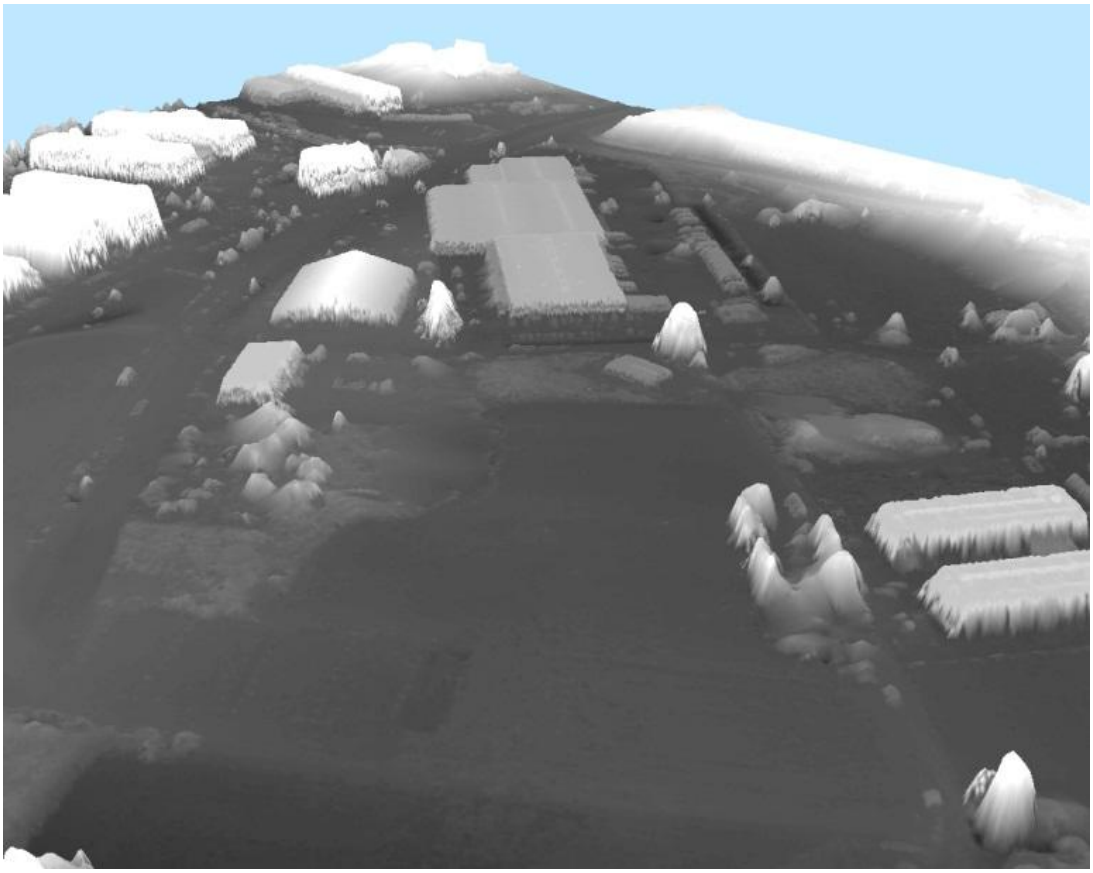

Figure 8 – Bloodhound DSM rendered in 3D

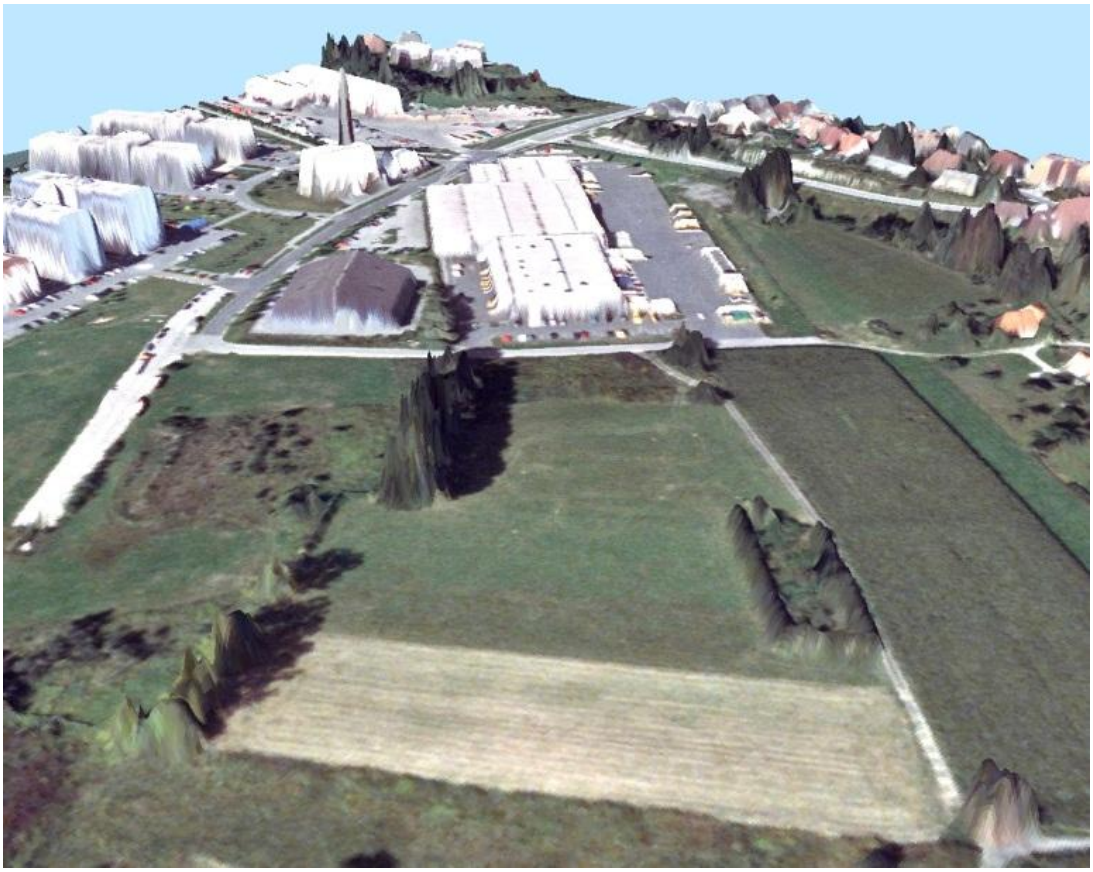

Figure 9 – LiDAR Orthomosaic rendered in 3D using LiDAR DSM elevations

Figure 10 – Bloodhound Orthomosaic rendered in 3D using Bloodhound DSM elevations

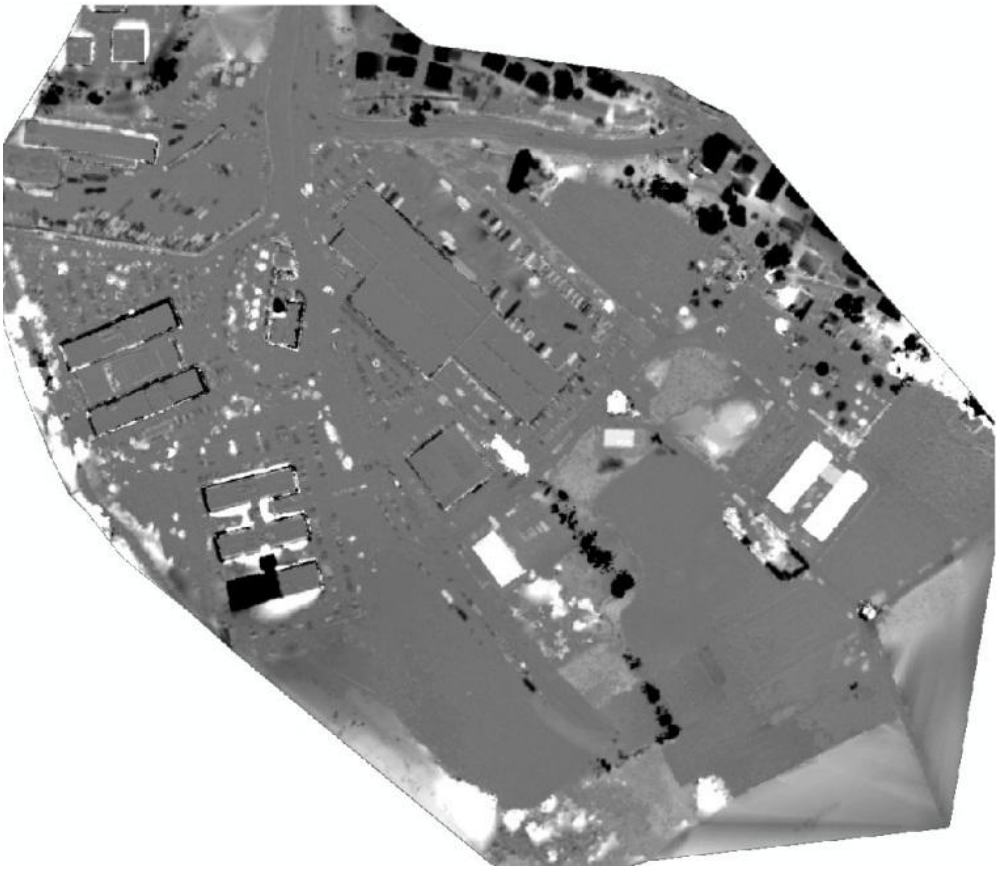

Figure 11 – Elevation differences between LiDAR and Bloodhound DSMs

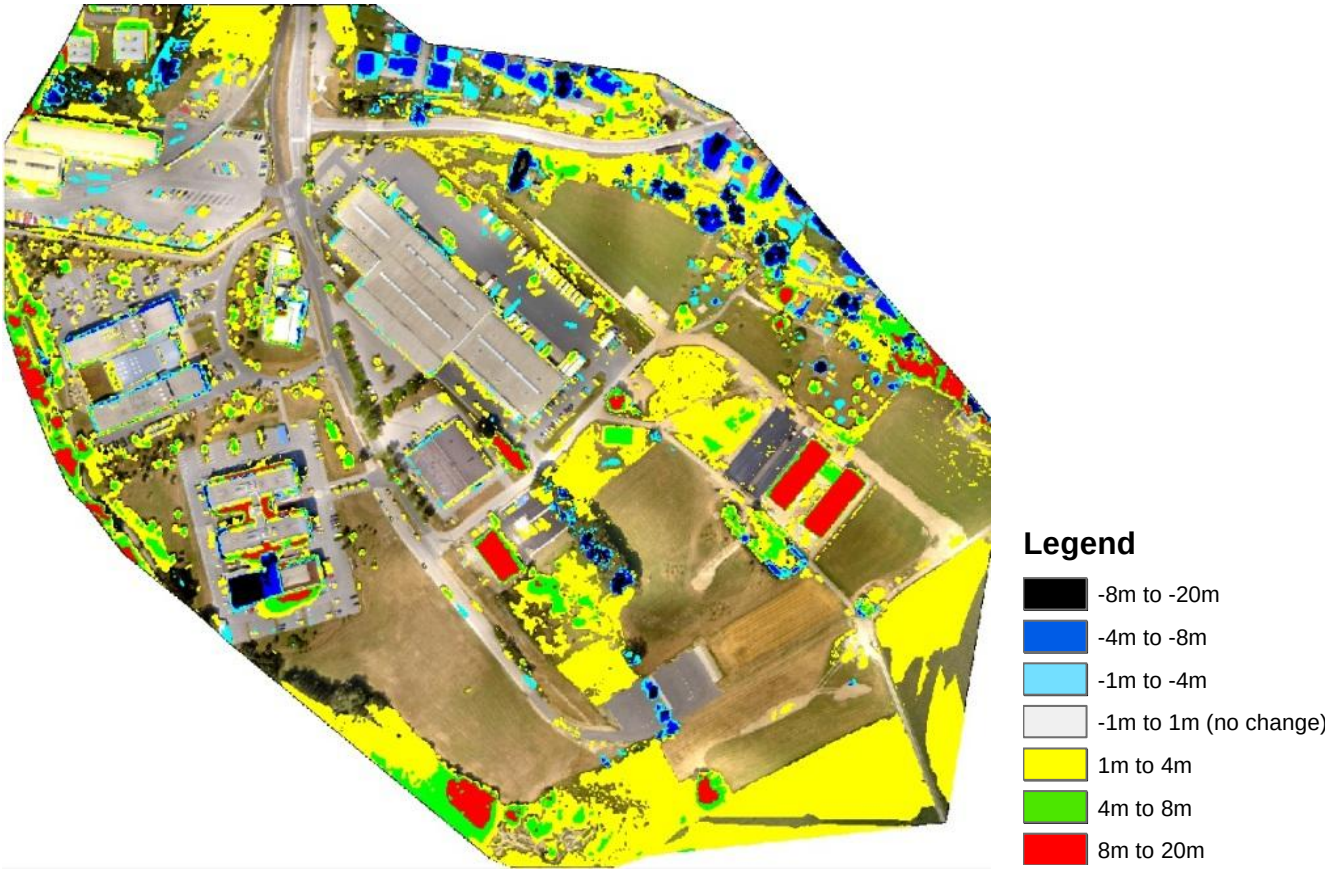

Figure 12 – Six Class Change Map over Bloodhound Mosaic (See Table 5)

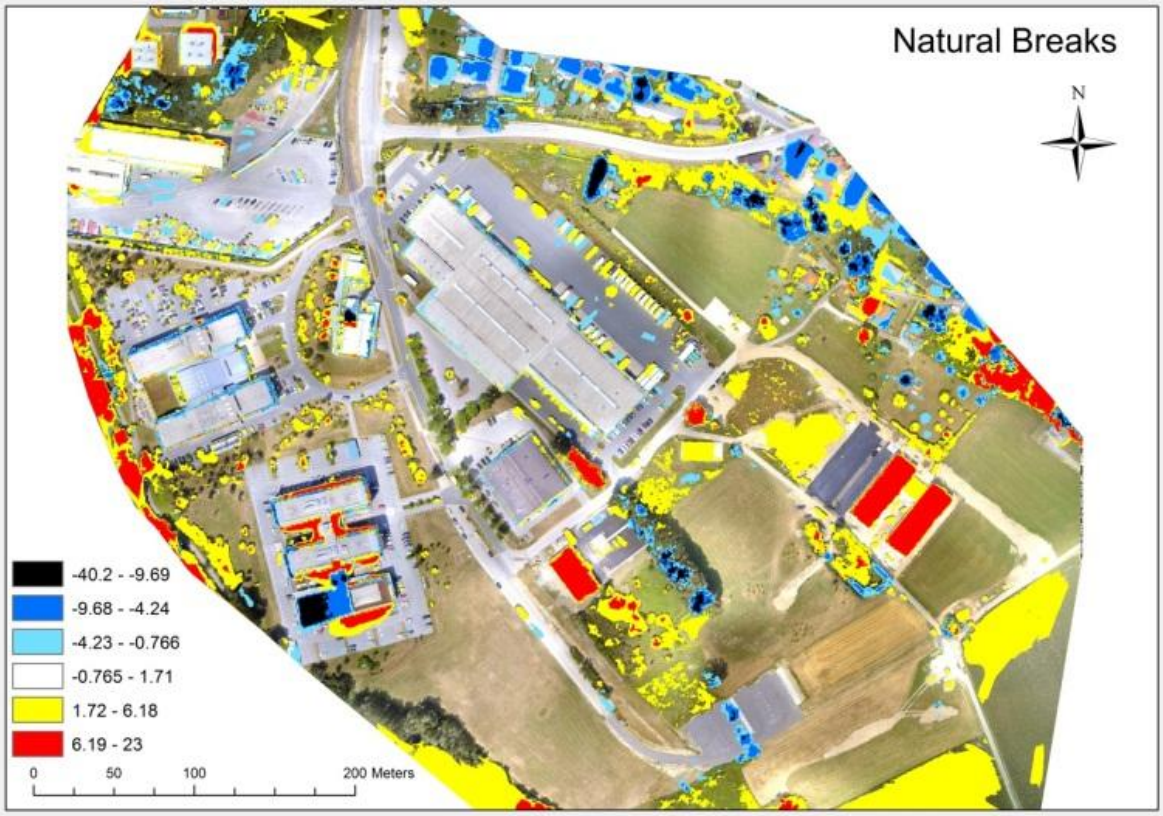

Figure 13 – Change Map over Bloodhound Orthomosaic using Natural Breaks (Jenks)

Figure 14 - Color Stretch Change Map using Difference DSM

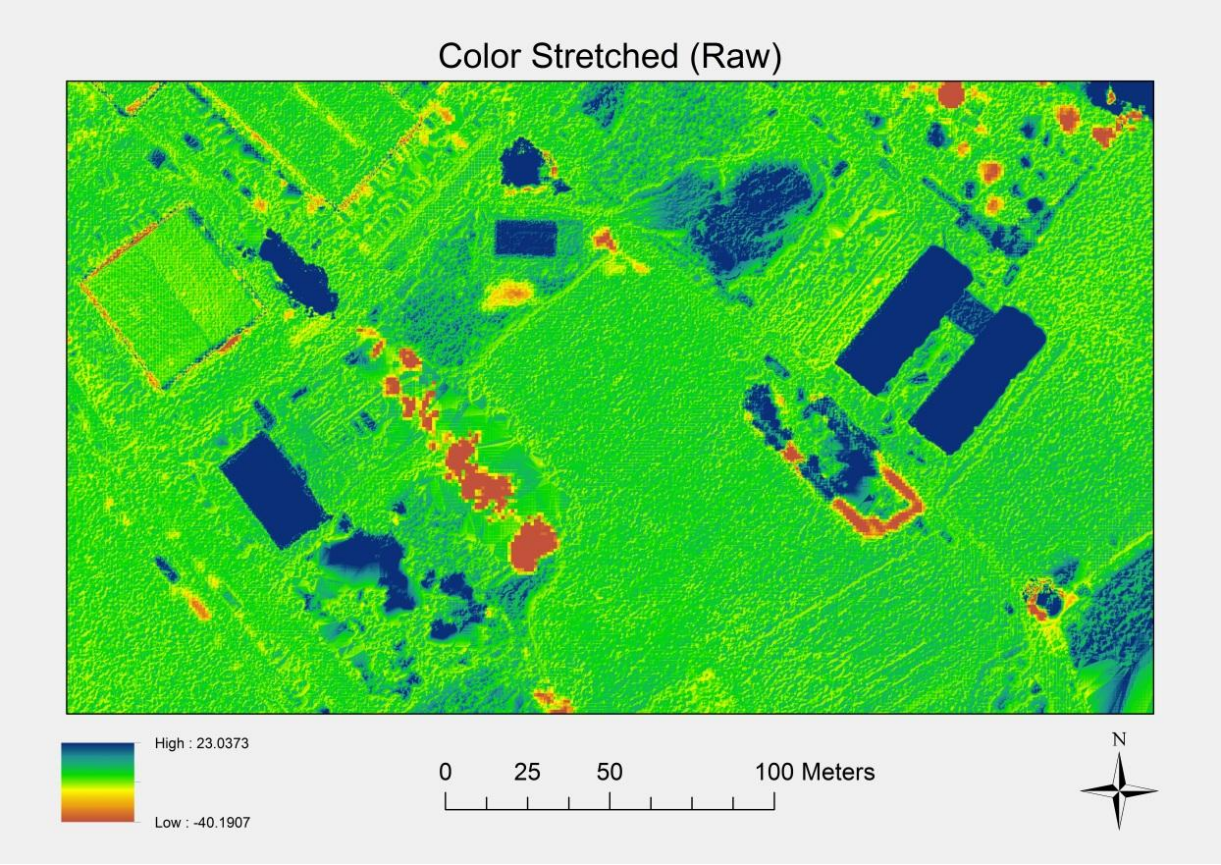

Figure 15 - Color Stretch Change Map focused on primary area of interest

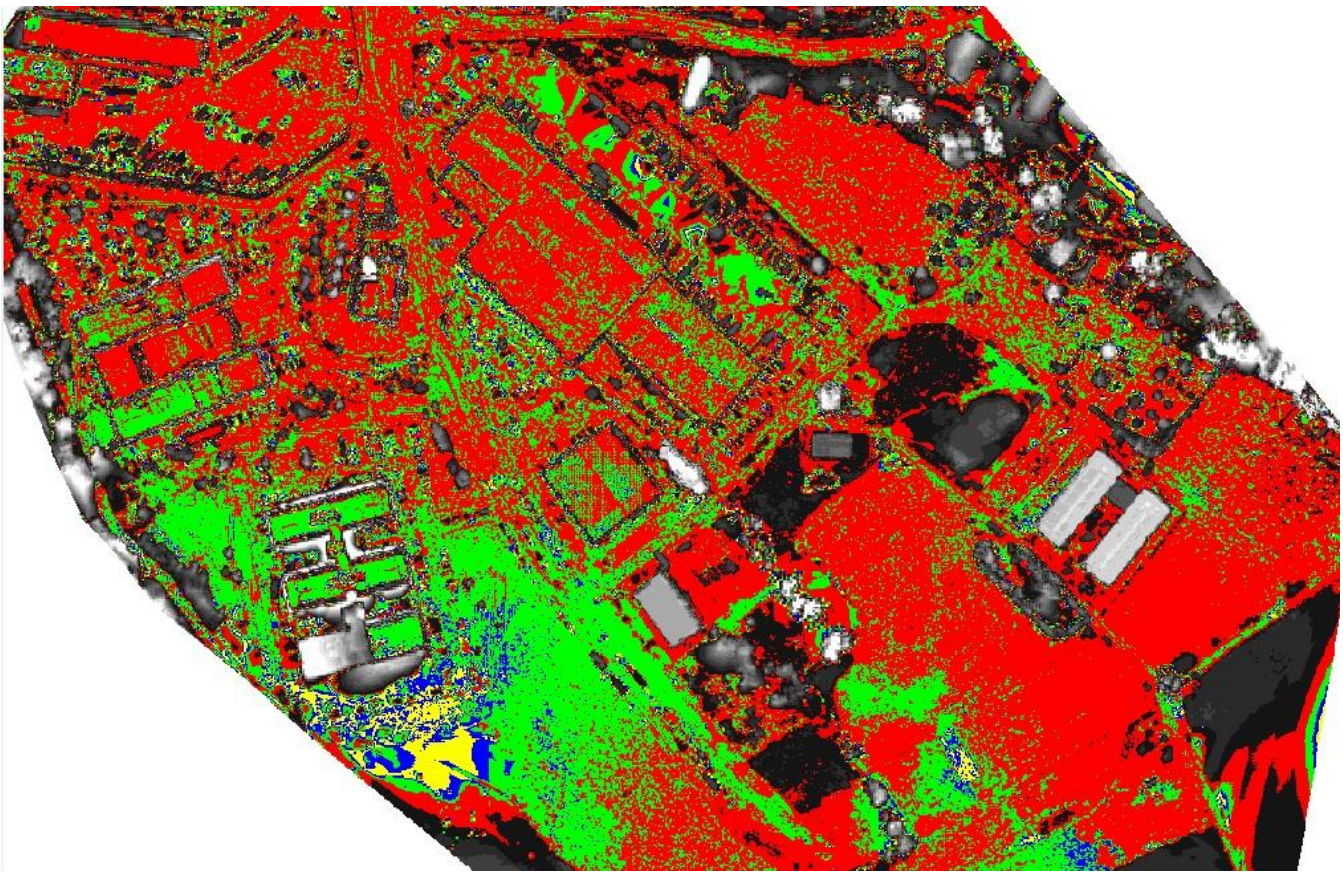

Figure 16 – Sub-meter Change mask. Red = 0.5m-1.0m, Green = 0.25m-0.5m, Blue = 0.1m-0.25m, Yellow = 0m-0.1m

Table 3 - Elevation Comparisons (meters)

GPS Point #	GPS Z	LiDAR Z	Bloodhound Z	Difference DSM Z
6 (Ground level)	538.979	538.577	538.985	0.225
46 (CUAS Roof)	554.826	553.885	554.67	0.582
48 (CUAS Upper Roof)	557.853	556.56	557.877	0.5

Table 4 - Building Height Comparisons (meters)

Structure	GPS Height	LiDAR Height	BH Height	Range Finder	Max Difference
CUAS Roof	15.847	15.308	15.685	15.758	0.539
CUAS Upper Roof	18.874	17.893	18.892	18.754	0.981
Dormitory	N/A	N/A	9.942	9.935	0.007
New Building	N/A	N/A	8.076	8.012	0.064
BSRTU	N/A	N/A	3.421	3.451	0.03

Table 5 - Six Class Change Mask Statistics (See Figure 13)

Class	Range (m)	Pixel Count	% Cover
1	-1 to 1 (no change)	38,627,611	69.235
2	1 to 4	11,762,653	21.083
3	4 to 8	1,632,679	2.926
4	8 to 20	1,115,871	2.000
5	-4 to -1	1,383,630	2.480
6	-8 to -4	848,361	1.521
7	-20 to -8	421,549	0.756

VIII. Discussion

Figures 4 through 10 depict original datasets before change detection processing and figures 11 through 16 provide various visual change detection products. Tables 3 through 5 provide statistical analysis of the results.

A visual analysis of the original datasets indicates that there are some inherent errors in the Bloodhound DSM, mostly around the perimeter. This is likely a result of extreme oblique angles in much of the input imagery as well. Additionally, the perimeter imagery of the flight block only has sidelap in one direction, so Bloodhound has less information available to construct the DSM in that area. A comparison of the lidar and Bloodhound DSMs rendered in 2.5-D using ArcScene 10 makes many changes in the terrain apparent. Draping the orthomosaics over their respective DSMs provides visual cues to the nature of these changes.

Figure 11 represents the difference image, or the raw, per-pixel elevation difference between the lidar and Bloodhound DSMs. Black areas indicate a negative elevation change

from the lidar to the Bloodhound DSM while white indicates a positive elevation change and grey indicates no (or negligible) change. Some buildings (like CUAS) have black borders around them indicating discrepancies between DSMs, while other buildings are completely black (north-east residential neighborhood) indicating that they were not generated in the Bloodhound DSM. A portion of the building south of CUAS was not constructed by the Bloodhound DSM properly either, due to its proximity to the perimeter and lack of adequate imagery. Bloodhound also had trouble constructing the large smoke-stack by CUAS as it does not appear in the Bloodhound DSM. Disregarding the anomalies, there are several new structures that appear in the difference image as well as changes in vegetation/tree canopy. A focused view of these structures and vegetation changes can be seen in Figure 15.

Another consideration to make when analyzing the change results is that the lidar and Bloodhound DSMs have different spatial scales. Lidar pixels have a 1 meter XY resolution while the Bloodhound pixels have approximately a 6.8 centimeter resolution, meaning that there are approximately 216 pixels in the Bloodhound DSM for every single pixel in the lidar. Coupled with Bloodhound's erratic generation of some building edges due to high oblique angles in the input imagery, many of the building borders in the difference image register as false changes. Anomalies resulting from this spatial discrepancy can be avoided in future research by comparing datasets with similar spatial resolutions.

Table 3 provides a comparison of raw elevation data between the lidar data, Bloodhound data, and GPS points. This data was useful in formulating the change mask parameters by providing an indication of the error margin in the datasets. The range of error between sampled points is 0.23 m to 0.58 m with an average of 0.44 m. Table 4 is comprised of building height readings from various sources. All readings are within 1 m accuracy with the largest being the upper portion of CUAS in the lidar vs the GPS reading with 0.98 m of difference. All sampled building heights in the Bloodhound DSM are within 0.2 m of height readings taken with a Leica laser range finder. These observations match the accuracy assessment performed by Küng et al. (2011). For the new (changed) structures, Bloodhound readings are within 0.007, 0.064 and 0.03 meters of the readings taken by the laser range finder. This indicates that Bloodhound's construction of these buildings in the DSM is extremely accurate. This is doubly impressive due to the fact that GPS points were collected only at ground elevations nearby.

The greatest discrepancies in building heights occur between the lidar data and the GPS/Bloodhound data. An initial response might be to claim that the Bloodhound and GPS data are biased towards each other as some of the GPS points were included as GCPs in the creation of the Bloodhound DSM which invalidates their comparison vs. the lidar. However, the building heights collected with the laser range finder also match the GPS and Bloodhound data much

more closely than they do the lidar. These observations imply that Bloodhound constructed sampled building profiles much more accurately that the lidar did. The counterpoint here is that the sampled buildings are all within the portion of the Bloodhound DSM that was adequately imaged by LOUIS with high overlap, near-nadir imagery.

In addition to new infrastructure, vegetation elevation change is also of interest. While there is no concrete, empirical data to support it, a visual analysis of the surface models and mosaics reveals some interesting observations. The DSM difference product (Figure 11) indicates numerous stark changes in vegetation (tree copses). Two of them can be seen in greater detail in Figure 15. Of the two distinct changes that appear in Figure 15, one indicates the complete removal of a stand of trees while the other indicates a new stand of trees. By comparing Figures 9 and 10, it can be see that, in fact, neither stand of trees has changed significantly between the two years. The first stand of trees (near the CUAS construction lab) was not detected by the lidar. The second stand of trees (just south east of the first) was not detected by Bloodhound. A third stand of trees further south east from the second stand was correctly identified as having been removed between the two datasets. This indicates that detection of vegetation elevation change is unreliable between these two datasets.

Table 5 provides a statistical analysis of the Six Class Change Mask depicted in Figure 12. Using this change mask, 69% of the landscape remained unchanged with regard to elevation while 21% of the landscape changed between 1 and 4 meters. 2% of the image changed between 8 and 20 m in the positive direction, most of which can be attributed to the construction of new infrastructure. A small part of this change however, is a result of the false change detection brought on by the lidar's omission of the first stand of trees. The 0.76% change of -8 to -20 m can be safely assumed to be majorly comprised of internal error in the Bloodhound data due to inadequate image coverage of said features. This includes the large smokestack, perimeter infrastructure and the second stand of trees south east of the CUAS construction lab. With so many anomalies inherent in the original data, much of this spatial statistical analysis is not as useful as visual interpretation and individual statistical analyses of known change quantities.

It is not uncommon for research projects to deviate from the original plans. Data collection can go awry, data processing techniques can work insufficiently or not at all, and results can invalidate a theory. This particular research project had a hiccup of its own during DSM and orthomosaic generation. The first snag arose during data processing. The original plan was to use ERDAS Leica Photogrammetry Suite (LPS) 2011 to generate a DSM from collected UAV imagery with the eATE terrain generation tool. Before LPS can begin terrain generation, the imagery has to be set up as a block with the appropriate parameters including interior camera parameters, exterior sensor orientations, and image geotags. The first error

arose with LPS's interpretation of exterior sensor orientations. LPS requires a very specific format for exterior orientation parameters such as omega, phi and kappa angles. Directifi's exterior orientation parameter export did not match LPS's required format. Additionally, Directifi did not provide enough information regarding the acquisition of exterior orientation parameters to convert them to the necessary format. As a result, image spatial footprints were extremely skewed and images that should have been overlapping were defined as looking opposite directions as can be seen in Figure 17.

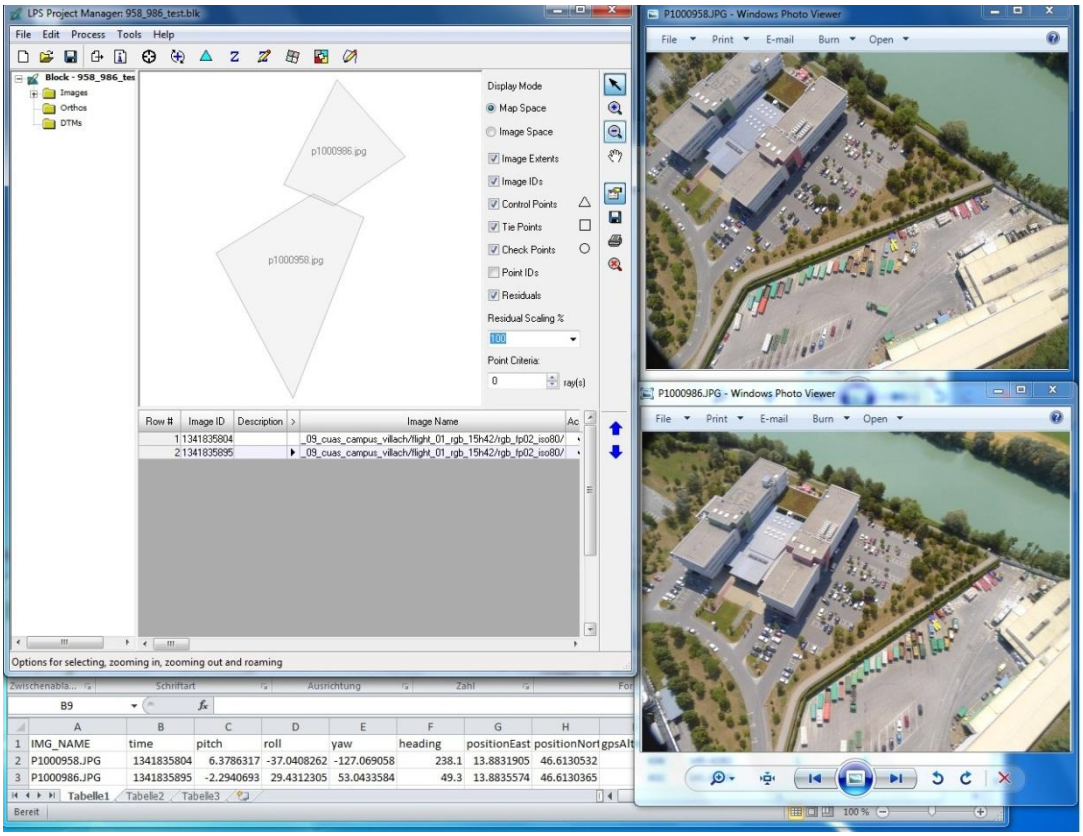

Figure 17 - Two overlapping images misinterpreted by LPS

The second snag arose shortly after with LPS's tie point generation. In order to complete triangulation and DSM generation, LPS must generate tie points between images in the block to tie the images together spatially and produce accurate results. The system running LPS did not have enough processing power to generate sufficient tie points across the large block of imagery. Even when the block of imagery was reduced to 12 images to test the method, LPS had trouble generating accurate tie points. Even if the system had the processing power to generate tie points across the full block of imagery, the accuracy of those generated points would not be sufficient to generate a DSM. However, a significant portion of LPS's inability to generate accurate tie points can likely be attributed to the incorrect interpretation of exterior sensor parameters and resulting skewed image spatial footprints. A block of this size

(approximately 140 images) requires thousands of tie points to successfully run. Generating these tie points automatically proved unsuccessful and generating them by hand would be unrealistic. The shortcomings of LPS forced a change of methods and the switch to Bloodhound, developed by Pix4D, to cloud process the imagery into a DSM and orthomosaic.

IX. Conclusions and Future Research

The research question for this project asked if accurate elevation change detection can be performed on airborne lidar using a digital surface model constructed from low altitude, digital camera, UAV imagery with automated photogrammetry techniques? The answer is yes, it can, but with caveats. This research demonstrated that accurate elevation change detection *can* be performed between lidar and photogrammetrically generated, low-altitude digital imagery, but the accuracy of the change detection will only be as good as the original data.

In areas where the UAV collected dense, near-nadir imagery, elevation change detection of infrastructure was highly accurate, but vegetation elevation change detection was hit-or-miss. In areas where the collected UAV imagery is less dense and highly oblique, elevation change detection becomes less reliable as Bloodhound's construction of the DSM becomes less accurate. Fortunately, the UAV imagery collected over the target change features was dense and near-nadir providing an accurate assessment of elevation change.

One major avenue for future research would be to analyze the rate of deterioration of the Bloodhound DSM as overlap decreases and sensor view-angles increase. Is the relationship between overlap and view-angle linear with DSM quality, or perhaps exponential? The results of this study seem to initially point towards an exponential relationship as the quality decreases drastically beyond a certain threshold seeing as the DSM is highly accurate in the center and highly inaccurate near the perimeter. Another potential future research opportunity would be attempting to improve the efficacy of detection elevation changes in vegetation using these methods. Within the focus area of this study, three stands of trees were detected as undergoing major change. Two of these, however, were a result of internal error in both datasets while one was correctly identified. Thus, it seems that the problem lies in accurately detecting vegetation elevations (both with lidar and automated photogrammetric techniques) rather than an inherent problem in the change algorithm.

Another substantial research opportunity generated from this study involves updating lidar datasets with elevation information gathered from DSMs generated from automatic photogrammetry techniques. Lidar is expensive to collect and if existing lidar data sets could be updated with information gathered using these UAV techniques, it would substantially reduce

the costs of having to acquire subsequent new lidar datasets for various studies. Existing lidar sets could be updated to reflect new infrastructure.

This research presents myriad new opportunities in GIS and remote sensing for utilizing low cost, UAV imaging to generate accurate terrain data. These terrain datasets can be used for disaster relief, monitoring urban expansion, urban planning, and potentially even forest and vegetation monitoring if vegetation can be accurately detected and constructed in the DSMs generated by these techniques. Datasets with comparable spatial resolutions (i.e. two DSMs generated with Bloodhound from imagery with similar scales) could even be used to compute volumetric change analysis. The questions are out there, it's just a matter of choosing which ones to answer.

X. References

Ambrosia, V. G., Wegener, S. S., Sullivan, D. V., Buechel, S. W., Dunagan, S. E., Brass, J. A., Stoneburner, J., et al. (2003). Demonstrating UAV-Acquired Real-Time Thermal Data over Fires. *Photogrammetric Engineering & Remote Sensing*, 69(4), pp. 391-402.

American Society of Photogrammetry (1980). Photogrammetric Engineering and Remote Sensing XLVI. 10, pp. 1249

Bruzzone, L., & Prieto, D. (2000). Unsupervised Change Detection. *IEEE Transactions on Geoscience and Remote Sensing, 38*(3), pp. 1171-1182.

Campbell, J., (1996). *Introduction to Remote Sensing.* New York, NY: The Guilford Press.

Coppin, P., and Bauer, M., (1996). Digital Change Detection in Forest Ecosystems with Remote Sensing Imagery. *Remote Sensing Reviews, 13*, pp. 207-234.

Corbane, C., Saito, K., Dell'Oro, L., Bjorgo, E., Gill, S., Piard, B.,…Eguchi, R., (2011). A comprehensive analysis of building damage in the 12 January 2010 Mw7 Haiti earthquake using high resolution satellite- and aerial imagery. *Photogrammetric Engineering and Remote Sensing 77*(10), pp. 997-1009.

Eisenbeiss, H. (2004). A Mini Unmanned Aerial Vehicle (UAV): System Overview and Image Acquisition. *International Workshop on Processing and Visualization Using High-Resolution Imagery*, 18-20 November, 2004, Pitsanulok, Thailand, pp. 1-7.

Eisenbeiss, H., Baltsavias, E., Pateraki, M., Zhang, L., (2004). Potential of IKONOS and QUICKBIRD Imagery for Accurate 3D-Point Positioning, Orthoimage and DSM Generation. *IAPRS. Vol 35 (B3)*, pp. 522-528.

Erdas, Inc., (2010). LPS Project Manager. User's Guide.

Everaerts, J., (2008). The Use of Unmanned Aerial Vehicles (UAVs) for Remote Sensing and Mapping. *The International Archives of the Photogrammetry, Remote Sensing and Spatial Information Sciences, 37*(B1), pp. 1187-1192.

Gehrke, S., Morin, K., Downey, M., Boehrer, N. and Fuchs, T. (2010). "Semi-Global Matching: An Alternative to LIDAR for DSM Generation?" *Canadian Geomatics Conference and Symposium of Commission I, ISPRS*, June 2010, Calgary, Canada.

Hussain, E., Ural, S., Kim, K., Fu, C., and Shan, J., (2011). Building Extraction and Rubble Mapping for City Port-au-Prince Post-2010 Earthquake with GeoEye-1 Imagery and Lidar Data. *Photogrammetric Engineering and Remote Sensing, 77*(10), pp. 1011-1023.

Jensen, J., (2007). Photogrammetry. In K. Clark (Ed.), Remote Sensing of the Environment (pp. 149-192) Upper Saddle River, NJ: Pearson Prentice Hall.

Kennedy, R., Townshend, P., Gross, J., Cohen, W., Bolstad, P., Wang, Y., Adams, P., (2009). Remote sensing change detection tool for natural resource managers: Understanding concepts and tradeoffs in the design of landscape monitoring projects. *Remote Sensing of Environmnent, 113*, pp. 1382-1396.

Küng, O., Strecha, C., Beyeler, A., Zuffrey, J-C., Floreano, D., Fua, P., Gervaix, F., (2011). The Accuracy of Automatic Photogrammetric Techniques on Ultra-Light UAV Imagery. *International Archives of the Photogrammetric, Remote Sensing and Spatial Information Sciences*, XXXVIII, pp. 1-6.

Laliberte, A. S., & Rango, A. (2009). Texture and Scale in Object-Based Analysis of Subdecimeter Resolution Unmanned Aerial Vehicle (UAV) Imagery. *IEEE Transactions on Geoscience and Remote Sensing, 47*(3), pp. 761-770.

Malila, W., (1980), Change vector analysis: An approach detecting forest changes with Landsat. *Proc. 6th Int. Symp. on Machine Processing of Remotely Sensed Data*, Purdue University, West Lafayette, Indiana, pp. 326-335.

Milne, A., (1988), Change direction analysis using Landsat imagery: A review of methodology. *Proc. IGARSS'88 Symp. (ESA SP-284),* Edinburgh, Scotland, pp. 541-544

Radke, R., Andra, S., Al-Kohafi, O., & Roysam, B., (2005). Image Change Detection Algorithms: a Systematic Survey. *IEEE Transactions on Image Processing, 14*(3) pp. 294-307

Rosin, P., (2002). Thresholding for change detection. *Computer Vision Image Understanding*, 86(2), pp. 79–95.

Rosin, P., and Ioannidis, E., (2003). Evaluation of global image thresholding for change detection. *Pattern Recognition Letters*, *24*(14), pp. 2345–2356

Singh, A., (1989). Digital change detection techniques using remotely-sensed data. *International Journal of Remote Sensing, 10*(6), pp. 989-1003.

Smits, P., and Annoni, A., (2000). Toward specification-driven change detection. *IEEE Transactions on Geoscience and Remote Sensing* 38(3), pp. 1484–1488

Strecha, C., (2011). Automated Photogrammetric Techniques on Ultra-Light UAV Imagery. *Pix4D, http://www.pix4d.com/downloads/pix4uav_accuracy.pdf*, pp. 1-11.

Strecha, C., Van Gool, L., Fua, P., (2008). A Generative Model for True Orthorectification. *The International Archives of the Photogrammetry, Remote Sensing and Spatial Information Sciences*, XXXVII, pp. 303-308.

Triggs, B., McLauchlan, P., Hartley, R., and Fitzgibbon, A., (2000). Bundle Adjustment – a Modern Synthesis. *Vision Algorithms: Theory and Practice*, pp. 298-372.

Touzi, R., (2002). A review of speckle filtering in the context of estimation theory. *IEEE Transactions on Geoscience and Remote Sensing, 40*(6), pp. 2392-2404.

Townshend, J., Justice, C., Gurney, C., McManus, J., (1992). The Impact of Misregistration on Change Detection. *IEEE Transactions on Geoscience and Remote Sensing, 30*(5), pp. 1054-1060

Wegener, S., and Schoenung, S., (2005). Lessons Learned from NASA UAV Science Demonstration Program Missions. *American Institute of Aeronautics and Astronautics*.

Woodcock, C., and Strahler, A., (1987). The factor of scale in remote sensing. *Remote Sensing of Environment, 21, pp. 311-332.*

Zitova, B., & Flusser, J. (2003). Image registration methods: a survey. *Image and Vision Computing*, *21*(11), pp. 977-1000.